# FORWARD FLIGHT STABILITY CHARACTERISTICS FOR COMPOSITE HINGELESS ROTORS WITH REFINED AEROELASTIC MODEL

Sung Nam Jung*
*Department of Aerospace Engineering*
*Chonbuk National University, Chonju 561-756, Republic of Korea*

Kyung Nam Kim, Chang Heon Han, Seung Jo Kim
*Department of Aerospace Engineering*
*Seoul National University, Seoul 151-742, Republic of Korea*

## Abstract

In this work, the aeroelastic stability behavior of composite hingeless rotor blade in forward flight is investigated by using the finite element method. The hingeless rotor model has soft-in-plane blade configurations and is Froud-scaled to match overall dynamic properties of full-scale helicopter rotors. The effects of transverse shear, torsion warping, and inplane elasticity are incorporated in the structural formulation. The shear correction factors capable of describing the coupling behavior of bending-shear and extension-shear are introduced here to consider the distribution of shear across the section of a composite blade. The aerodynamic model in the current aeroelastic analysis is formulated to allow either quasi-steady or unsteady two-dimensional aerodynamics. Compressibility and reversed flow effects on the blade are also incorporated. Numerical simulations are carried out to validate the current approach and to show the influence of elastic couplings on the aeroelastic stability solutions. The effects of unsteady aerodynamic models and geometric design variables such as precone, taper, and pretwist on the stability behavior of composite hingeless blade are also studied in detail.

## Introduction

Generally, the aeroelastic analysis for the composite rotor blade is performed through the one-dimensional beam assumption. Even though many simplifying assumptions can be drawn in the beam model, the key factors for obtaining accurate analysis results are to capture effectively a number of nonclassical effects, such as transverse shear and warping, in the beam kinematics. Hong and Chopra[1] used a simple kinematic model of a composite beam to examine the effects of elastic couplings on the aeroelastic stability in hover. The beam model did not consider the transverse shear couplings of bending-shear and extension-shear. Rehfield et al.[2], addressed the importance of nonclassical behavior for the thin-walled composite beams. They showed that the effect of transverse shear flexibility is independent of the slenderness of the beam due to the existence of the elastic coupling between bending and shear deformations. Fulton and Hodges[3] studied the stability behavior of elastically tailored composite rotor in hover and showed some results regarding the importance of including the nonclassical couplings. The structural analysis is based on a mixed finite element representation of geometrically exact nonlinear beam theory[4], and aerodynamic analysis is based on a quasi-steady lift model.

Torok and Chopra[5] investigated the stability behavior of an isotropic hingeless rotor blade in forward flight with nonlinear unsteady aerodynamic model based on the work of Leishman and Beddoes[6]. They showed that the unsteady aerodynamic effects can significantly improve the regressive lag mode damping estimations. Smith and Chopra[7] developed a direct analytical approach to examine the elastic coupling behavior of composite beams and analyzed the dynamics of a hingeless rotor in forward flight by including the transverse shear, cross section warping, and in-plane ply elasticity. A shear flexible 19 DOF beam finite element was developed in the analysis, but they did not consider the distribution of shear in the beam cross section. Quasi-steady aerodynamic theory with compressibility and reversed flow effects was used to obtain the aeroelastic response of the rotor. The linear attached flow unsteady aerodynamics on the blade response and vibratory hub load were also studied.

* Currently, Post-doctoral Fellow at Center for Rotorcraft Education and Research, Univ. of Maryland, U.S.A.

None of the authors in our knowledge, however, have been tried unsteady aerodynamic effects on the aeroelastic stability of composite rotor blade.

Jung and Kim[8,9] investigated the effects of transverse shear and structural damping on the aeroelastic response of stiff-in-plane composite helicopter blade in hover. They introduced the shear correction factor (SCF) to account for the sectional distribution of shear and improved the prediction of dynamic response of composite rotor. They showed that the effects of transverse shear and structural damping can have a key role on the flutter boundary of the rotor, but the flight envelope of the analysis was confined to hover and the SCF used was calculated from the formula of an isotropic thin-walled box section. Recently, Kim et al.[10] studied the stress distributions across rectangular and thin-walled box sections, and determined the SCF for the sections by imposing the equality of shear deformation energies with taking into account of bending-shear and extension-shear couplings.

In this paper, the aeroelatic stability of a composite hingeless blade in forward flight is investigated. The rotor model has soft-inplane blade configurations and is Frould-scaled to match overall dynamic properties of MBB BO-105[11]. The structural model is based on the work of Jung and Kim[8] which includes the effects of transverse shear, torsion warping, and inplane elasticity behavior. The formula of SCF driven by Kim et al. is used to consider the distribution of shear across the composite beam section. The aerodynamic model is formulated to allow either quasi-steady or unsteady two-dimensional aerodynamics. Compressibility and reversed flow effects are also incorporated. The objective of the research work is 1) to establish a consistent analysis method to capture the nonclassical structural effects of composite beams like transverse shear capable of describing bending-shear and extension shear couplings, and 2) to investigate the elastic coupling behavior of the composite hingeless blade in forward flight with special emphasis on the unsteady aerodynamic model. Finally, the effects of rotor blade design parameters such as precone, pretwist, and taper on the aeroelastic stability of composite rotor are studied.

## Formulation

Fig.1 shows the schematic of the elastic blade whose structure is represented as a single-cell laminated composite box-beam. Several coordinate systems are used to describe the blade motion : the $X_H$-$Y_H$-$Z_H$ hub-fixed nonrotating coordinate system, $X$-$Y$-$Z$ hub-rotating coordinate system, the $x$-$y$-$z$ undeformed coordinate system and the $\xi$-$\eta$-$\zeta$ deformed coordinate system. The undeformed blade coordinate system x-y-z is attached to the undeformed blade which is at a precone angle of $\beta_p$ in the hub-rotating coordinate system. The deformation of a point on the blade is described by the displacements $u$, $v$, $w$, and $\varphi$, which are respectively axial, lead-lag, flap, and elastic twist deformations. The total transverse displacements $v$ and $w$ for lead-lag and flap bendings are expressed as the sum of the displacements due to bending and the displacement due to shear deformation[8].

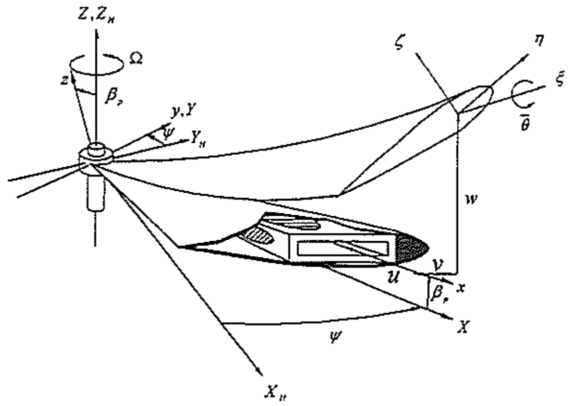


**Fig. 1 Rotor blade geometry and coordinate systems.**

The strain-displacement relations for small strains and moderately large deformations up to second order can be obtained in the following form as

$$\begin{aligned}
\varepsilon_{xx} &= u' + \frac{v_b'^2}{2} + \frac{w_b'^2}{2} - \lambda_T \phi'' + (\eta^2 + \zeta^2)(\theta_0' \phi' + \phi'^2/2) \\
&\quad - v_b''(\eta \cos\bar{\theta} - \zeta \sin\bar{\theta}) - w_b''(\eta \sin\bar{\theta} + \zeta \cos\bar{\theta}) \\
\gamma^t_{x\eta} &= -(\zeta + \frac{\partial \lambda_T}{\partial \eta})\phi' \\
\gamma^t_{x\zeta} &= (\eta - \frac{\partial \lambda_T}{\partial \zeta})\phi' \\
\gamma^s_{x\eta} &= \{v_s' \cos\bar{\theta} + w_s' \sin\bar{\theta}\}\, f_1(\eta, \varsigma) \\
\gamma^s_{x\zeta} &= \{w_s' \cos\bar{\theta} - v_s' \sin\bar{\theta}\}\, f_2(\eta, \varsigma)
\end{aligned} \tag{1}$$

where subscript $b$ refers to bending deformation and subscript $s$ refers to shear deformation, $\lambda_T$ is the St. Venant warping function, and $f_1$, $f_2$ are arbitrary functions with sectional coordinates $\eta$ and $\zeta$. In the strain-displacement relations, the total shear strain components, $\gamma_{ij}$, are composed of torsion-related strain components, $\gamma^t_{ij}$, and transverse-shear-related strain components, $\gamma^s_{ij}$.

In order to perform the aeroelastic analysis of a composite rotor with maintaining one-dimensional beam kinematics, the functions, $f_1$ and $f_2$, are to be modified in suitable forms, because the beam has parabolic distribution of shear in the beam cross section[10]. Unless corrected for the functions, three dimensional beam modeling is required for the analysis and is not desirable to conduct formidable aeroelastic calculations. The first-order shear deformation theory is adopted in the present beam formulation to consider this sectional distribution of shear. After all, the functions $f_1$ and $f_2$, which are corresponds to SCF's, have constant values. In case of composite beam section, the shear correction coefficients are functions of the geometry and the material property of the beam. Kim et al.[10] studied the distribution of shear for the generally orthotropic beam having rectangular and thin-walled box sections and formulated the equation of SCF for the sections by using the equality of shear deformation energies obtained in two cases: assumed constant shear strain and actual shear strain. The formula of SCF driven by Kim[10] is used in the present beam formulation.

The constitutive relations of horizontal and vertical laminae of box-beam walls have respectively the following form

$$\begin{Bmatrix} \sigma_{xx} \\ \sigma_{x\eta} \end{Bmatrix} = \begin{bmatrix} C_{11} & C_{16} \\ C_{16} & C_{66} \end{bmatrix} \begin{Bmatrix} \varepsilon_{xx} \\ \gamma_{x\eta} \end{Bmatrix}$$
$$\begin{Bmatrix} \sigma_{xx} \\ \sigma_{x\zeta} \end{Bmatrix} = \begin{bmatrix} C_{11} & C_{16} \\ C_{16} & C_{66} \end{bmatrix} \begin{Bmatrix} \varepsilon_{xx} \\ \gamma_{x\zeta} \end{Bmatrix} \tag{2}$$

where the stiffness coefficients $C_{ij}$ are defined by applying the plane stress assumption for the laminates as

$$C_{ij} = \overline{Q}_{ij} - \frac{\overline{Q}_{i2}\overline{Q}_{2j}}{\overline{Q}_{22}} \quad \text{for } i,j = 1, 6 \tag{3}$$

where the expressions for the transformed reduced stiffness matrix $\overline{Q}_{ij}$ in terms of material constants are given in Jones[12].

The governing differential equations of motion for the composite hingeless rotor blade in forward flight can be derived by using the Hamilton's energy principle

$$\int_{t_1}^{t_2} (\delta U - \delta T - \delta W_e)dt = 0 \tag{4}$$

where $\delta U$, $\delta T$, and $\delta W_e$ are strain energy variation, kinetic energy variation, and external virtual work done, respectively, and they are defined as

$$\delta U = \int_0^R \iint_A (\sigma_{xx}\delta\varepsilon_{xx} + \sigma_{x\eta}\delta\gamma_{x\eta} + \sigma_{x\zeta}\delta\gamma_{x\zeta})dAdx \tag{5}$$

$$\delta T = \int_0^R \iint_A \rho V \cdot \delta V \, dAdx \tag{6}$$

$$\delta W_e = \int_0^R [\, L_u\delta u + (L_{v_b} + L_{v_s})(\delta v_b + \delta v_s) + (L_{w_b} + L_{w_s})(\delta w_b + \delta w_s) + M_\phi \delta p \,] \; dx \tag{7}$$

where $A$ is the cross section of the blade and $R$ is the blade length. In the kinetic energy expression (6), $V$ is the velocity vector for a given point on the deformed frame, and $\rho$ is the density of blade. In the right hand side of the virtual work equation (7), $L_u$ and $M_\phi$ are the aerodynamic force and moment distributed along the length of the blade in axial and twist directions, $L_{v_b}$ and $L_{v_s}$ denote the edgewise components of aerodynamic forces in bending and shear parts, and $L_{w_b}$ and $L_{w_s}$ denote the flapwise components of aerodynamic loades in bending and shear deformations, respectively. The aerodynamic forces and moments in the equation (7) are determined about the elastic axis in the deformed blade frame. The $\delta p$ is the virtual rotation of of a point on the deformed elastic axis of the beam. In order to calculate the external aerodynamic loads on the rotor blade, both quasi-steady and unsteady strip theories are used. This unsteady aerodynamic model has been developed by Leishman and Beddoes[6] and is based on an indicial response method which uses Duhamel's superposition integral. The effects of compressibility and reversed flow are also incorporated in the aerodynamic models. Components of non-circulatory origin aerodynamics are also included in the variational equation. Drees linear inflow model is used for the distribution of steady induced inflow.

Applying the finite element method to Hamilton's principle, one can get the nonlinear finite element equations of motion in terms of nodal degrees of freedom $q$ in a matrix form as

$$\mathbf{M}\ddot{\mathbf{q}} + \mathbf{C}(\mathbf{q},\psi)\dot{\mathbf{q}} + \mathbf{K}(\mathbf{q},\psi)\mathbf{q} = \mathbf{F}(\psi,\mathbf{q},\dot{\mathbf{q}}) \tag{8}$$

where $M$, $C$, $K$, and $F$ are the global inertia, damping, stiffness matrices, and load vector respectively. The damping and stiffness matrices have asymmetric nature due to the influence of nonconservative aerodynamic forces and moments, and are functions of azimuth angle in the rotor disc plane. The blade structure is discretized into a number of beam finite elements. Each beam element is composed of two end nodes and three internal nodes , which results in a total of 23 degrees of freedom per element including eight transverse shear degrees of freedom to fully consider the flap-lag-torsion behavior of the rotor.

The solution of the governing differential equations of motion (8) requires first the determination of the blade equilibrium conditions. In order to reduce computation time required to obtain the steady responses of the blade, modal superposition technique is applied to the finite element equations. The rotating free vibration analyses for the modal vectors are performed priori to transform the system mass, damping, and stiffness matrics to modal space. The modal equations of motion for the response solution can be written as

$$\overline{\mathbf{M}}\ddot{\mathbf{r}}+\overline{\mathbf{C}}(\psi)\dot{\mathbf{r}}+\overline{\mathbf{K}}(\mathbf{r},\psi)\mathbf{r}=\mathbf{Q}_{nl}(\psi,\mathbf{r},\dot{\mathbf{r}}) \tag{9}$$

where the over bar of the system matrices means that the matrices are resulted from modal coordinate transformations. All the nonlinear terms are put in the load vector $\boldsymbol{Q}_{nl}$ for convenience. The global nodal variables $\boldsymbol{q}$ can be obtained from the modal coordinates $\boldsymbol{r}$ using the transformation as

$$\mathbf{q}=\Phi\mathbf{r} \tag{10}$$

where $\Phi$ is a modal matrix which is determined from rotating free vibration analysis. The nonlinear, periodic normal mode equations (9) are solved for equilibrium responses using a finite element method in time[13]. For this solution, the time period of one rotor revolution is discretized into a series of time finite elements as for the blade in space domain. Periodic boundary conditions are imposed on the initial and final states of the blade in the time domain.

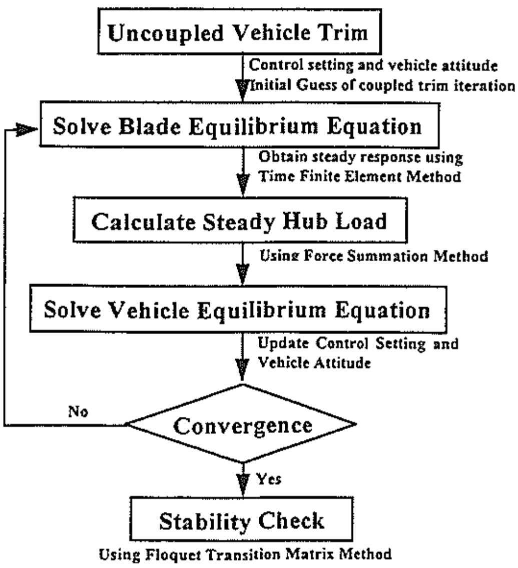


**Fig. 2 Solution procedures.**

A coupled trim procedure as used in Ref. 14 is adopted to obtain the blade deflections, pilot inputs (collective and cyclic), and vehicle orientation simultaneously. The coupled trim analysis in forward flight consists of calculation of vehicle propulsive trim, blade steady deflections, and hub forces and moments. The propulsive trim involves three force equations (vertical, longitudinal, and lateral) and three moment equations (pitch, roll, and yaw). The propulsive trim solution is used as an initial guess for the blade equilibrium equation and iterated through updating of hub forces and moments in the coupled trim algorithm as demonstrated in Fig. 2. Force summation method is used to obtain the hub loads in the rotating blade frame, and Fourier coordinate transformations are applied to calculate the hub loads in the hub-fixed nonrotating frame. In the coupled trim iteration, the blade steady deflections and vehicle trim parameters are converged at once within a given tolerence value.

After performing the coupled trim iterations, the stability analysis of the blade is followed from the linearized perturbation equations about the trimmed positions. This linearized flutter equations are transformed to the modal space in a first order form. The transformed modal flutter equations are solved as an algebraic eigenvalue problem with periodic coefficients by using the Floquet transition matrix theory as discussed in Dugundji et al.[15].

## Results and Discussions

### Comparison Results

The structural dynamic behavior of rotating composite box-beams having symmetric and antisymmetric configurations had been correlated in the previous work[8] with other experimental data[16]. Before going directly to the aeroelastic calculations, the present forward routines must be checked and validated. The article of Smith and Chopra[7] presented perhaps the most advanced solutions up to this time for the forward flight aeroelastic stability of composite rotor blade. Figure 3 shows the comparison results of steady tip deflections with respect to azimuthal variations between the present results and the data of Smith et al. for a soft-inplane four bladed rotor at forward speed $\mu$ =0.3 and thrust ratio $C_T/\sigma$ =0.07. The model rotor properties used in the calculations are listed in Ref. 7. Fairly good correlations are obtained for the steady responses as depicted in Fig. 3. In Fig. 4, the variation of lead-lag damping is plotted versus flight speed $\mu$ for the two results. Despite the different formulations and solution schemes used in the two

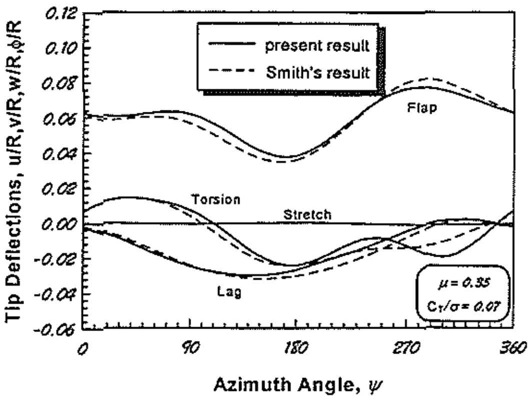


**Fig. 3 Comparison results for steady tip deflections at forward speed $\mu$ =0.35.**

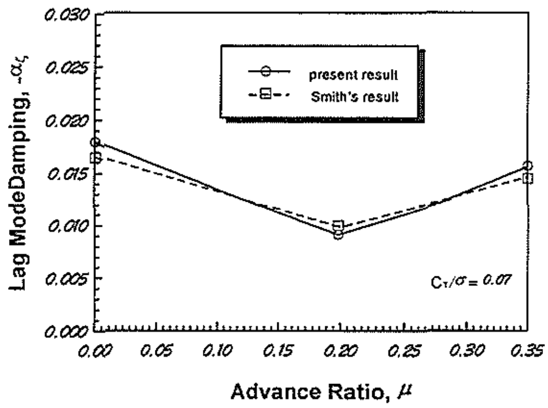


**Fig. 4 Comparison of stability results with forward speed.**

approaches, excellent correlation is obtained.

## Elastic and Geometric Coupling Effects

Numerical simulations for the aeroelastic stability of a soft-inplane helicopter blade with elastically coupled rotor blade are carried out by using the rotor model of Weller[11] which is Froude-scaled to match overall dynamic properties of production hingeless rotors with emphasis on the MBB BO-105. Rotor model geometric and operational properties are summarized in Table 1. The materials used are for the AS4-3501-6 graphite-epoxy lamina and the mechanical properties are: $E_1$=20.59 msi, $E_2$=1.42 msi, $G_{12}$=0.87 msi, and $\nu_{12}$=0.42. The rotor structure is carefully designed to yield realistic values of rotating natural frequencies: fundamental lag frequency $\nu_\zeta$=0.7, fundamental flap frequency $\nu_\beta$=1.12, and first torsional frequency $\nu_\phi$ =5.0. The model rotor configurations are categorized into seven cases: baseline uncoupled configuration,

**Table 1. Model rotor properties.**

| Property | Value |
|---|---|
| Rotor Radius, $R$, in | 52.8 |
| Chord, $c$, in | 3.70 |
| Rotor Speed, $\Omega$, rpm | 660 |
| Lock No. $\gamma$ | 6.5 |
| Solidity Ration, $\sigma$ | 0.089 |
| Thrust Ratio, $C_T/\sigma$ | 0.08 |
| Hub Vertical Offset, $h/R$ | 0.2 |
| C.G. Offset, $X_{cg}/R$, $Y_{cg}/R$ | 0., 0. |
| Hub Length, $x_{hub}/R$ | 0.015 |
| Hub Precone, $\beta_p$ | -5° |
| Blade Pretwist, $\theta_0'$ | 1° |
| Mass per Unit Length, $m$, slug/ft | 0.00866 |
| Flat Plate Area, $f/\pi R^2$ | 0.01 |
| Tail Rotor Radius, $r_{tr}/R$ | 0.2 |
| Tail Rotor Solidity, $\sigma_{tr}$ | 0.15 |
| Tail Rotor Location, $x_{tr}/R$ | 1.2 |
| Tail Rotor above c.g., $h_{tr}/R$ | 0.2 |
| Horizontal Tail Location, $x_{ht}/R$ | 0.65 |
| Horizon Tail Area, $S_{ht}/\pi R^2$ | 0.008 |

pitch-lag coupled (symmetric A and B), pitch-flap coupled (symmetric C and D), and tension-pitch coupled configurations(anti-symmetric A and B). The baseline blade exhibits no elastic couplings and has a cross ply layup. Table 2 shows the configuration details for the layup geometry used in the study. The symmetric case A exhibits positive pitch-lag couple (lag back - pitch down) and symmetric case C exhibits positive pitch-flap couple (flap up - pitch down). The anti-symmetric case A has positive tension-pitch couple (tension - pitch down). The other pairs for the layup configurations in Table 2 have negative couplings.

The stability results for the pitch-lag coupled configurations with increasing forward speeds are presented in Fig. 5. The elastic couplings are shown to play a significant role on the lag mode stability. The negative pitch-lag coupling (symmetric B) is stabilizing compared to the baseline uncoupled configuration, while the positive pitch-lag coupling (symmetric A) is destabilizing. In the symmetric B configuration, the change of damping with varying flight speeds is very large compared to the symmetric A configuration. Though not notable, the stability margins of symmetric A case are increased with flight speeds. The lag damping results for the symmetric C and D cases are presented in Fig. 6. Symmetric C case (positive pitch-flap couple) is destabilizing, while symmetric D case (negative pitch-flap couple) is stabilizing. The amount of damping magnitudes is not large in comparison with the results of Fig. 5.

Table 2. **Different composite box-beam configurations.**

| | *Top* | *Bottom* | *Left* | *Right* |
|---|---|---|---|---|
| ***Baseline uncoupled*** | $[90/0]_{2s}$ | $[90/0]_{2s}$ | $[90/0]_{2s}$ | $[90/0]_{2s}$ |
| ***Symmetric A*** | $[90/0]_{2s}$ | $[90/0]_{2s}$ | $[30_2/(90/0)_3]$ | $[30_2/(90/0)_3]$ |
| ***Symmetric B*** | $[90/0]_{2s}$ | $[90/0]_{2s}$ | $[-30_2/(90/0)_3]$ | $[-30_2/(90/0)_3]$ |
| ***Symmetric C*** | $[30_2/(90/0)_3]$ | $[30_2/(90/0)_3]$ | $[90/0]_{2s}$ | $[90/0]_{2s}$ |
| ***Symmetric D*** | $[-30_2/(90/0)_3]$ | $[-30_2/(90/0)_3]$ | $[90/0]_{2s}$ | $[90/0]_{2s}$ |
| ***Anti-Symmetric A*** | $[-30_2/(90/0)_3]$ | $[30_2/(90/0)_3]$ | $[-30_2/(90/0)_3]$ | $[30_2/(90/0)_3]$ |
| ***Anti-Symmetric B*** | $[30_2/(90/0)_3]$ | $[-30_2/(90/0)_3]$ | $[30_2/(90/0)_3]$ | $[-30_2/(90/0)_3]$ |

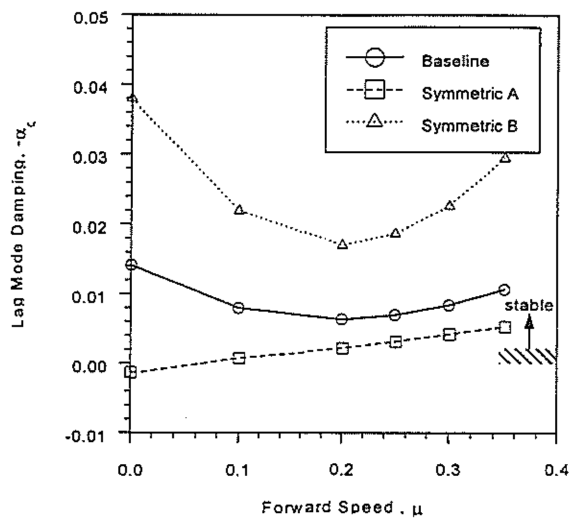


**Fig. 5 Lag mode damping for symmetric A and B configurations with flight speed $\mu$.**

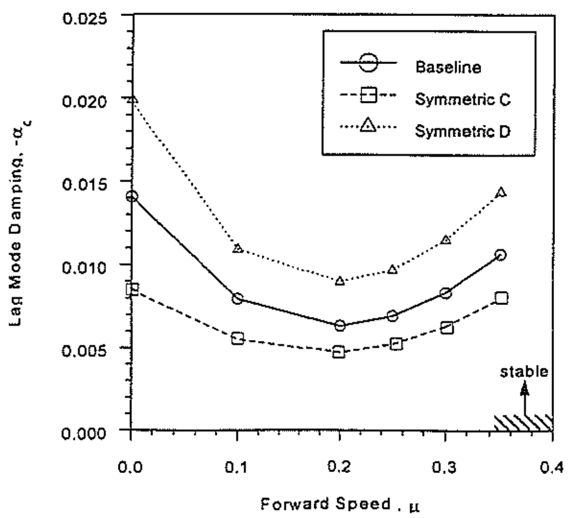


**Fig. 6 Lag mode damping for symmetric C and D configurations with flight speed $\mu$.**

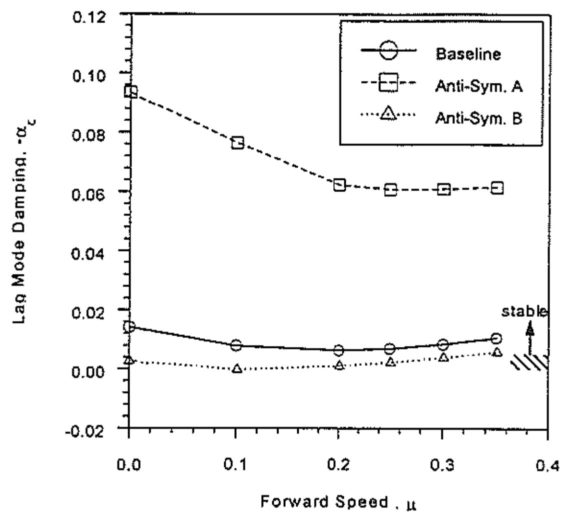


**Fig. 7 Lag mode damping for antisymmetric configurations with flight speed $\mu$.**

The beneficial effects of elastic tailoring are demonstrated in good fashion for the cases of antisymmetric configuration as depicted in Fig. 7. Positive tension-pitch couple (antisymmetric A) presented strong stabilizing effects on the blade. The amount of lag mode damping increases more than five times as much as for the baseline blade configuration. But, for the antisymmetric B case (tension - pitch up couple), the blade becomes less stable than the baseline case.

As can be seen from Table 1, the small-scale rotor model uses hub precone and blade pretwist angles for the blade. These angles are frequently used in recent blade designs to relax hub loads and to smooth the aerodynamic lift distributions over span of the blade, respectively. In Fig. 8, the effects of precone on the lag mode damping for the composite blade are presented. Precone angles are varied as 0°, 1°, 3°, and 6° for the study. The baseline model rotor has precone angle of 1°. As a whole, the introduction of precone is shown to increase the lag mode

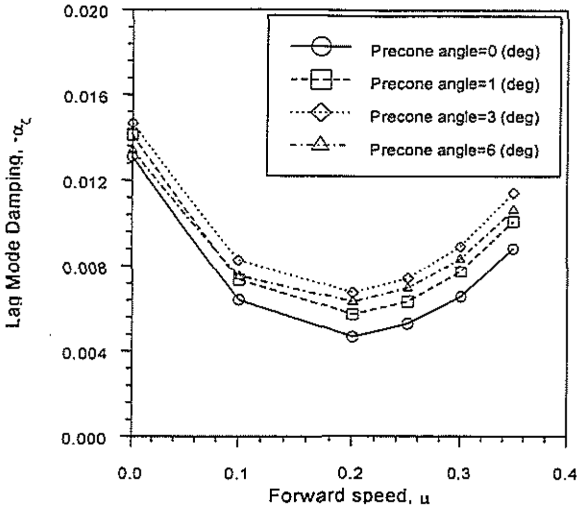


**Fig. 8 Effects of precone on the lag mode stability with flight speeds.**

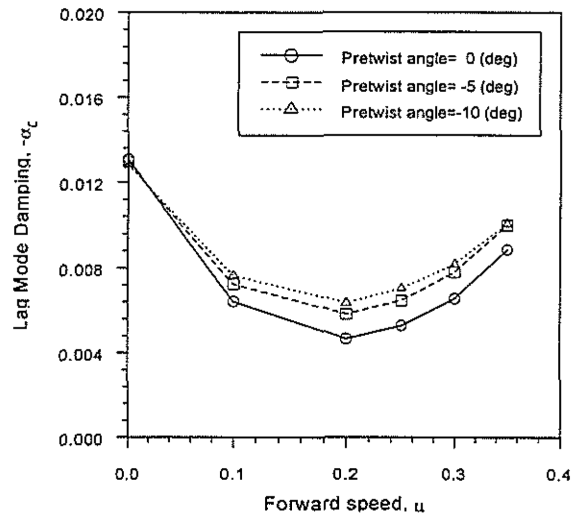


**Fig. 9 Effects of pretwist on the lag mode stability with flight speeds.**

damping for overall flight ranges, but the magnitude of damping is upper bounded near precone angle of 3°. The effects of pretwist on the lag mode stability with flight speeds are plotted in Fig. 9. The stabilizing trends by pretwist angles are obvious as seen in the figure.

Fig. 10 shows the taper effects on the lag mode damping with a function of flight speed. Results are calculated for a helicopter blade with a tapered planform at the tip. The taper begins at 80% of the rotor radius and decreases linearly towards the rotor tip without changing mass distribution. It is observed that, with the introduction of tip taper, the blade becomes less stable than the baseline untapered blade.

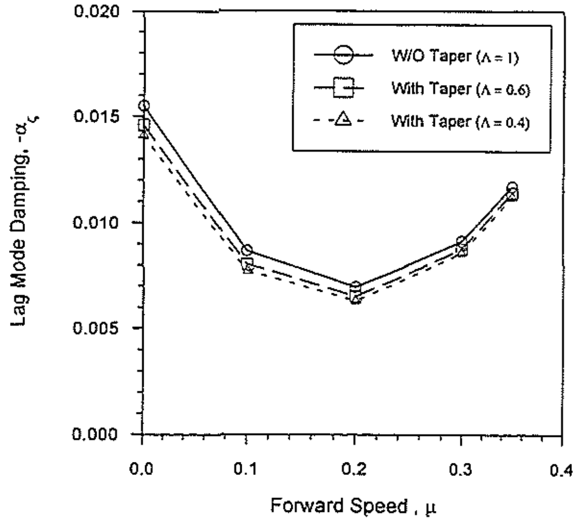


**Fig. 10 Effects of planform taper on the lag mode stability with flight speeds.**

## Unsteady Aerodynamic Effects

The effects of unsteady aerodynamics on the lag mode damping for a soft-in-plane hingeless rotor are addressed in this section. The vehicle properties are similar to the full-scale BO-105 hingeless design: rotor radius $R$ =193.7 *in*, Lock No. $\gamma$=7, solidity ratio $\sigma$=0.089, and hover tip Mach No. $M_{tip}$=0.673. In this time, three different laminate configurations are evaluated. The baseline blade exhibits no elastic coupling and each laminate of the all four box-beam walls has layup of $[(90/0)_5/(45/-45)_3/0_4]_s$. The left and right walls of the box-beam in case A configuration featuring positive pitch-lag coupling have layup of $[30_4/(15/-15)_3/(45/-45)_3/0_4]_s$, while symmetric case B is composed of $[-30_4/(15/-15)_3/(45/-45)_3/0_4]_s$ for the left and right walls of the box-beam, which exhibits negative pitch-lag couple. The layup geometry of top and bottom walls for the cases A and B is set as $[(90/0)_5/(45/-45)_3/0_4]_s$ not to present any pitch-flap types of couple.

The stability results for both the baseline and case A configurations with quasi-steady and unsteady aerodynamic theories are presented in Fig. 11. With the inclusion of positive pitch-lag couplings, gradual decrease of damping with flight speeds is observed. This is a consistent results as discussed in the previous section. Negative damping values are obtained at over flight speed of $\mu$ =0.2. Inclusion of unsteady aerodynamic effects has substantial influence on the predicted lag mode damping as seen in the plot. Fig. 12 shows the lag mode stability results for the Case B configuration (negative pitch-

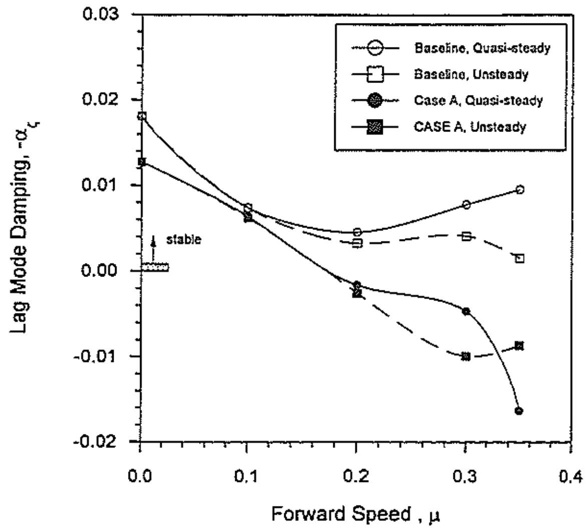


**Fig. 11 Unsteady aerodynamic effects on the lag mode stability with forward speeds.**

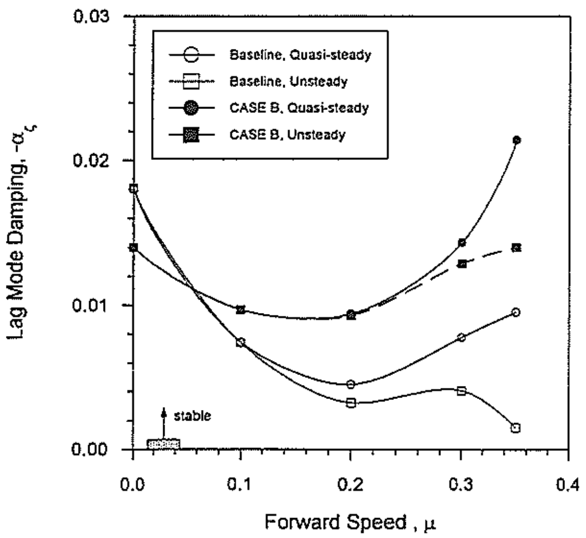


**Fig. 12 Unsteady aerodynamic effects for case B on the lag mode stability with forward speed.**

lag couple) with increasing flight speeds. The baseline uncoupled case is also inserted in the plot for comparison purpose. Stabilizing trends are clearly seen with the introduction of elastic couplings except hover and low forward speed regions. As can be seen in the figure, the unsteady effects get dominant at high forward speeds ($\mu$ >0.2) and the damping estimations becomes marginal as speeds up. This trends are also seen with increasing thrust ratio as presented in Fig. 13. At thrust level of $C_T/\sigma$=0.1, the unsteady case predicts negative damping, but still, the lag mode damping remains in the stable region for the quasi-steady case.

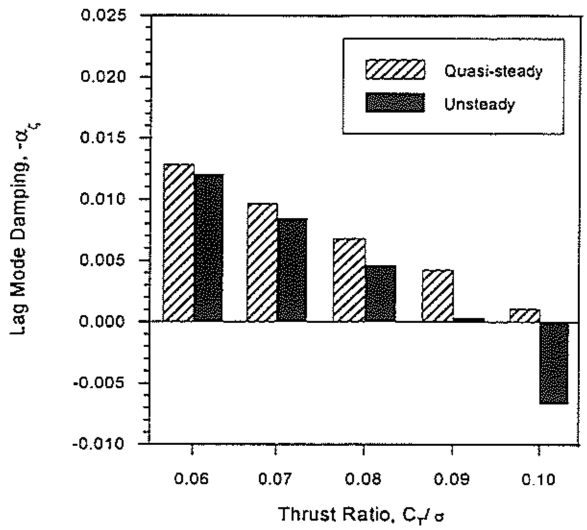


**Fig. 13 Effects of unsteady aerodynamic modeling on the lag mode stability with increasing thrust ratio $C_T/\sigma$.**

## Concluding Remarks

A finite element approach has been performed to investigate the effects of the elastic couplings and unsteady aerodynamics on the aeroelastic stability of composite hingeless rotor blade in forward flight. In the structural formulation, nonclassical effects of beam such as transverse shear and torsion warping are incorporated and the sectional distribution of shear across beam section considering bending-shear and extension-shear couplings is taken into account for the analysis. The aerodynamic model is formulated to allow either quasi-steady or unsteady two-dimensional aerodynamics. The unsteady aerodynamics are calculated using an indicial response method with Duhamel's superposition principle. From the current work, the following conclusions are drawn:

1) The present forward flight aeroelastic results for the steady blade responses and the lag mode stability solutions are compared and validated with other available analysis results.
2) The negative pitch-lag couple (lag back - pitch up) has a significant stabilizing effects on the blade and the negative pitch-flap couple (flap up-pitch up) stabilizes the lag motion slightly.
3) The antisymmetric layup blade with positive tension pitch coupling (tension-pitch down) demonstrated a great potential for aeroelastic tailoring: the amount of lag mode damping increases more than five times compared to baseline configuration.
4) Inclusion of unsteady aerodynamic effects has substantial influence on the lag mode stability

behavior and is prerequisite for enhanced aeroelastic solutions. The effects are enlarged with increasing forward speed and thrust ratio.

## References


1. Hong, C. H., and Chopra, I., "Aeroelastic Stability Analysis of a Composite Rotor Blade," *Journal of the American Helicopter Society*, Vol. 30, No. 2, Apr. 1985, pp. 57-67.
2. Rehfield, L. W., Atilgan, A. R., and Hodges, D. H., "Nonclassical Behavior of Thin-Walled Composite Beams with Closed Cross Sections," *Journal of the American Helicopter Society*, Vol. 35, No. 2, May 1990, pp. 42-50.
3. Fulton, M. V., and Hodges, D. H., "Aeroelastic Stability of Hingeless, Elastically Tailored Rotor Blades in Hover," *Proceedings of the Winter Annual Meeting of the American Society of Mechanical Engineers*, Anaheim, California, Nov. 8-13, 1992, pp. 9-23.
4. Hodges, D. H., "Mixed Variational Formulation Based on Exact Intrinsic Equations for Dyanmics of Moving Beams," *International Journal of Solids and Structures*, Vol. 26, No. 11, 1990, pp. 1253-1273.
5. Torok, M. S., and Chopra, I., "Hingeless Rotor Aeroelastic Stability Analysis with Refined Aerodynamic Modeling," *Journal of the American Helicopter Society*, Vol. 36, No. 4, Oct. 1991, pp. 48-56.
6. Leishman, J. G., and Beddoes, T. S., "A Semi-Empirical Model for Dynamic Stall," *Journal of the American Helicopter Society*, Vol. 34, No. 3, July 1989, pp. 3-17.
7. Smith, E. C., and Chopra, I., "Aeroelastic Response, Loads and Stability of a Composite Rotor in Forward Flight," *AIAA Journal*, Vol. 31, No. 7, July 1993, pp. 1265-1273.
8. Jung, S. N., and Kim, S. J., "Aeroelastic Response of Composite Rotor Blades Considering Transverse Shear and Structural Damping," *AIAA Journal*, Vol. 32, No. 4, April 1994, pp. 820-827.
9. Jung, S. N., and Kim, S. J., "Effect of Transverse Shear on Aeroelastic Stability of a Composite Rotor Blade," *AIAA Journal*, Vol. 33, No. 8, Aug. 1995, pp. 1541-1543.
10. Kim, S. J., Yoon, K. W., and Jung, S. N., "Shear Correction Factors for Thin-Walled Composite Boxbeam Considering Nonclassical Behaviors," *Journal of Composite Materials*, Vol. 30, No. 10, 1996, pp. 1133-1149.
11. Weller, W. H., "Relative Aeromechanical Stability Characteristics for Hingeless and Bearingless Rotors," *Journal of the American Helicopter Society*, Vol. 35, No. 3, July 1990, pp. 68-77.
12. Jones, R. M., *Mechanics of Composite Materials*, McGraw-Hill, New York, 1975.
13. Borri, M., "Helicopter Rotor Dynamics by Finite Element Time Approximation," Computers and Mathematics with Applications, Vol. 12A, No. 1, 1986, pp.149-160.
14. Lim, J. W., "Aeroelastic Optimization of a Helicopter Rotor," Ph. D. Dissertation, Univ. of Maryland, 1988.
15. Dugundji, J., and Wendell, J. H., "Some Analysis Methods for Rotating Systems with Periodic Coefficients," *AIAA Journal*, Vol. 21, No. 6, 1983, pp. 890-897.
16. Chandra, R., and Chopra, I., "Experimental-Theoretical Investigation of the Vibration Characteristics of Rotating Composite Box Beams," Journal of Aircraft, Vol. 29, No. 4, 1992, pp.657-664.